Molecular Therapy
Nucleic Acids
Original Article

Design of bifunctional RNA-binding compounds that can modulate siRNA hydrophobicity for deep penetration and gene silencing in the retina

Qi Mao,[1] Yanan Quan,[1] Siyi Chen,[2] and Wanyi Tai[1]

[1]Department of Pharmaceutical Engineering, School of Pharmaceutical Sciences, Wuhan University, Wuhan, Hubei 430071, China; [2]Department of Pharmacy, Zhongnan Hospital of Wuhan University, Wuhan, Hubei 430071, China

Small interfering RNA (siRNA) could be a promising new modality to block the neovascularization in retinal diseases. For ocular siRNA delivery, hydrophobic modification is essential to increase the siRNA membrane compatibility, self-deliverability, and retinal penetration. Current covalent approach such as cholesterol or fatty acid conjugation can only tether one hydrophobic ligand to siRNA molecule, which shows limitations in the ocular delivery. Here, we identified a siRNA-binding drug, quinacrine, and conjugated it with cholesterol to obtain a bifunctional RNA-binding compound that can act as a tag to tether multiple cholesterol molecules on siRNA non-covalently. Despite a moderate affinity to siRNA (K_D = 932 ± 26 nM), the tag can convert siRNA into a fully hydrophobic (logP = 1.86), membrane-permeable and self-deliverable (IC_{50} = 166 ± 59 nM) molecule. Tagged with a miniature and chemically modified anti-VEGF siRNA, a single intravitreal administration enables siRNA penetration of all retinal cell layers and induces effective gene silencing over 1 month in the mouse model. The data suggest that the bifunctional RNA-binding compound could be a useful small-molecule carrier to promote siRNA delivery in the retina.

INTRODUCTION

Angiogenesis in the retina is a root cause of several retinal diseases, including wet age-related macular degeneration (wAMD), diabetic retinopathy, retinopathy of prematurity, and retinal vein occlusion.[1] As the global causes of blindness, retinal diseases are a devastating burden to patients, and also the relatives who take care of them. The current mainstream treatment involves the intravitreal injection of anti-vascular endothelial growth factor (VEGF) medications to block the retinal angiogenesis. VEGF is a potent angiogenic factor that stimulates proliferation of vascular endothelial cells.[1] Its overexpression induces abnormal angiogenesis and vascular permeability, which ultimately led to the formation of choroidal neovascular membranes and the death of overlying photoreceptor cells.[2] Protein-based anti-VEGF inhibitors are the most common drugs in the clinical practice to treat retinal diseases.[3] The FDA-approved agents, including antibodies (ranibizumab, faricimab), their fragment scFv (brolucizumab), and Fc fusion proteins (aflibercept), can cover a market size of over 25 billion in 2025, as per analysis from Market Research Future Report.[4] Intravitreal injection is an accepted route to deliver protein drugs in the ocular site, but frequent injections (once every 4–6 weeks) are needed to maintain the therapeutic benefit.[5] Frequent injection poses a risk of ocular damage and intraocular inflammation; some can cause vision problems.[6] A practical approach is to use the higher dose or bigger injection volume that can contribute to extending the drug durability. For example, Bayer is sponsoring a phase 3 clinical trial (NCT04423718) to investigate the effect of high-dose aflibercept (8 mg every 12 weeks) as a long-term therapy to replace the standard 2 mg aflibercept for AMD therapy.[7] Despite the feasibility of dose scale-up, the maximum safe volume of intravitreal injection is only 50–100 μL, which limits the space for further optimization. Other approaches, such as intravitreal implant of devices, provide a longer duration of pharmacologic effect, but the ocular implant procedure is associated with patient reluctance.[8]

Besides protein inhibitors, siRNA could be a new modality to treat retinal diseases.[9] Different from VEGF blockers, siRNA can knock down VEGF expression via the RNA interference (RNAi) mechanism, which is well known for its high specificity and potency. When modified with advanced stabilization chemistry and Ikaria technology, siRNA has an extremely long duration of action *in vivo*, supporting even once yearly dosing in the clinical setting.[10] For example, phase 1 data revealed that ALN-TTRsc04 can maintain the transthyretin (TTR) reduction level >70% over 360 days following a single dose of 300 mg.[11] Owing to these advantages, siRNA has been proposed as a means to treat retinal diseases as early as the 2000s.[12,13] Bevasiranib and AGN211745 are the first two siRNA agents being evaluated in clinical trials for treating neovascular AMD.[14,15] Both agents were intravitreally injected in a naked siRNA form. However, siRNA is a highly hydrophilic macromolecule that has poor pharmaceutical properties. Without

Received 17 July 2025; accepted 17 October 2025;
https://doi.org/10.1016/j.omtn.2025.102751.

Correspondence: Wanyi Tai, Department of Pharmaceutical Engineering, School of Pharmaceutical Sciences, Wuhan University, Wuhan, Hubei 430071, China.
E-mail: wanyi-tai@whu.edu.cn

modification or carrier assistance, siRNA tends to be degraded, and unable to penetrate the cell membrane to access the RNAi machinery in the cytosol. Besides the plasma membrane barrier, ocular siRNA has to penetrate the complex retinal layers to reach cells expressing VEGF proteins. Likely due to difficulties posed by these barriers, the initial design faced various challenges and led to the termination of development around 2010.

Hydrophobic modification of siRNA is a promising strategy to solve the problem.[16] By conjugation with cholesterol, siRNA can display a certain degree of membrane compatibility and self-delivery ability.[17] Khvorova and colleagues upgraded the technology by cholesterylating an asymmetric siRNA that contains a single-stranded 5-bp tail for cellular internalization (to mimic the antisense oligonucleotide behavior).[18,19] It highlights an innovative hydrophobic siRNA with self-delivering ability and drug-like property, which can deliver locally to the skin, eye, and brain.[20] This technology was later licensed to RXi pharmaceuticals and termed "self-delivering rxRNA" (sd-rxRNA) for commercialization.[20] One of its pipelines, RXI-109, was studied in phase 2 clinical trials for the treatment of advanced neovascular AMD and accompanying subretinal fibrosis in 2018.[21] Despite the advances, no siRNA therapy has yet translated into patient care for retinal diseases. Albeit more hydrophobic than the naked siRNA, cholesterol-siRNA conjugates, including sd-rxRNA, have an amphiphilic structure. When it interacts with cells, the hydrophobic cholesterol tail might insert into the lipid bilayer, but the hydrophilic siRNA is blocked outside of the membrane, making permeation inefficient. Incorporation of more cholesterol to siRNA, especially at multiple positions to balance the distribution of hydrophobicity, would promote membrane permeation and penetration capability. Hydrophobicity and penetration might be especially important to the anti-VEGF siRNA in the ocular therapy, considering that the retina contains at least five cell layers and that all can produce VEGF proteins.[1] However, the extensive modification of siRNA could seriously attenuate its RNAi potency, and thus multiple cholesterylation by chemistry is not an applicable approach.

In this study, we reported that bifunctional RNA-binding compounds can modulate siRNA hydrophobicity by a conjugation-free methodology. The compound contains a cholesterol moiety and a siRNA-binding group that can attach around the siRNA backbone to make it hydrophobic, membrane permeable, and self-deliverable (Figure 1A). We have previously demonstrated the feasibility of this method using a cholesterol-ethidium tag.[22] With concerns regarding ethidium-induced genotoxicity, we here screened a library of >10 RNA-binding compounds to identify a functional and biosafe molecule for siRNA tagging. Here, FDA-approved drug quinacrine emerges as the lead because of its high affinity and good safety as an antimalarial agent in clinical use.[23] Anti-VEGF therapy using a miniature siRNA and quinacrine-based tag2 revealed that hydrophobic siRNA can penetrate deeply into mouse retinal layers and induce a gene-specific silencing effect. This study may open a new avenue for siRNA ocular delivery to treat retinal diseases.

RESULTS

Design of bifunctional compounds to modulate siRNA hydrophobicity

To design bifunctional molecules, we first need to identify an RNA-binding compound that can help tag cholesterols on the siRNA surface. The canonical siRNA is a typical short dsRNA (19–21 bp duplex) plus 2-nucleotide (nt) 3′ overhangs. As a dsRNA, siRNA exhibits a typical A-form configuration, which is distinct from the B-form DNA in helix width, length, and groove topography. Consequently, many well-known DNA dyes might not bind well with siRNA, especially those recognizing DNA grooves, for example, DAPI (4',6-diamidino-2-phenylindole). To identify a siRNA binder, we selected 12 chemical compounds from the literature or FDA-approved drug list (Drugbank database) based on their structure and likelihood to interact with siRNA bases. As shown in Figure 1A, they were selected because their planar aromatic structures may intercalate siRNA and form π-π stacking interactions with base pairs. To screen potential binders, their affinity to siRNA was measured using the Octet biolayer interferometry (BLI) assay. Briefly, the amino-modified siRNA was immobilized on the AR2G biosensor using the NHS reaction kit. A series of compound concentrations was probed against the immobilized siRNA on the sensor. The kinetics of compounds' association and dissociation to siRNA were recorded to calculate the K_D values. As shown in Figure 1B, most compounds demonstrated moderate avidities to siRNA, with K_D values ranging from 800 to 1,700 nM (BLI sensorgrams are available in Figure S1). Surprisingly, amoxapine and compound 2 fail to bind siRNA, albeit they have similar aromatic cores to clozapine (K_D = 1321 ± 153 nM) and quinacrine (K_D = 856 ± 25 nM). Compound 1 is an analog of acridine and possesses two protonable tertiary amines to interact with siRNA backbones as a bonus. However, it did not show a higher affinity to siRNA than acridine, indicating that the intercalation force by aromatic rings dominates the siRNA-compound interaction. By re-probing them against dsDNA, we found that most siRNA-binding compounds exhibit no selectivity between siRNA and dsDNA, with the exception of neomycin, which shows no affinity to dsDNA. This observation is in line with Arya et al.'s report that neomycin's preference is for A-form nucleic acids.[24] Despite the good selectivity of neomycin to siRNA, the bifunctional compound of neomycin was not pursued due to the scarcity of its binding sites (the major groove) on siRNA.[25]

Eight siRNA-binding compounds were functionalized with cholesterol for further evaluation. After cholesterylation, most of these compounds (tags) retain the binding ability to siRNA and dsDNA (Figure 1B). Moreover, cholesterylation dramatically reduces the cytotoxicity of some siRNA binders to the retinal pigment epithelia cell line ARPE-19 (Figures 1B and S2). For example, TAS-103, a DNA topoisomerase I/II inhibitor for cancer therapy, has high cytotoxicity to ARPE-19 (IC_{50} ∼0.002 μM) but its bifunctional tag (tag3) shows an IC_{50} value of ∼0.175 μM, which is 87.5 times higher

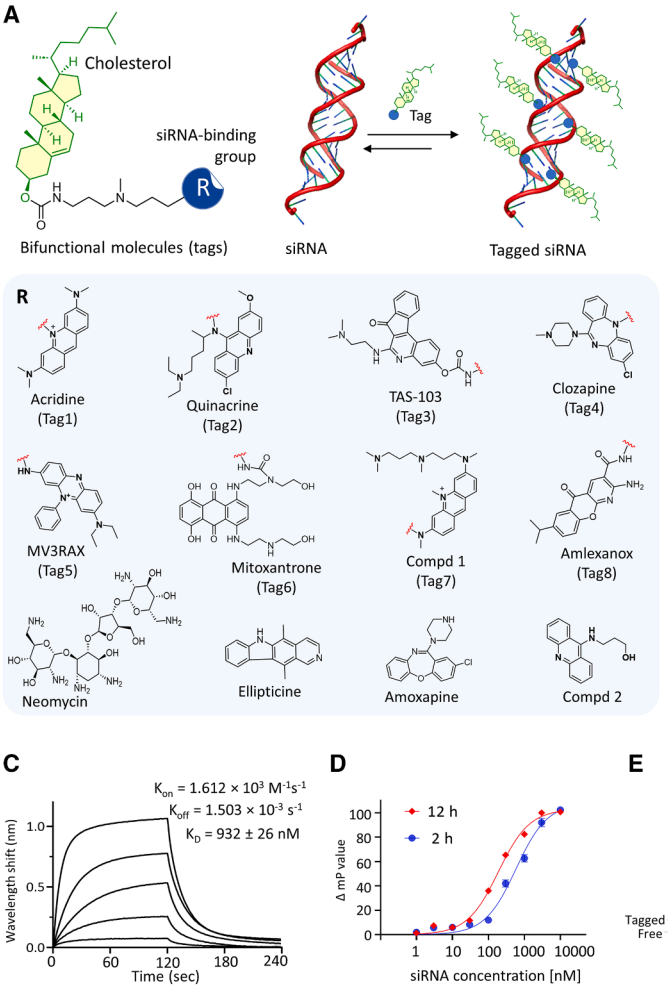

B

Compounds' affinity (BLI) and cytotoxicity test (CCK-8)

Compds	K_D (nM)		IC_{50} (μM)*
	siRNA	dsDNA	ARPE-19 cells
Acridine	916 ± 56	956 ± 31	2.526 ± 0.831
Quinacrine	856 ± 25	1163 ± 58	> 100
TAS-103	1777 ± 136	1217 ± 102	0.002 ± 0.0001
Clozapine	1321 ± 153	1254 ± 134	> 100
MV3RAX	1556 ± 128	1328 ± 145	0.423 ± 0.12
Mitoxantrone	1027 ± 121	998 ± 65	0.031 ± 0.012
Compd 1	1031 ± 85	908 ± 74	1.905 ± 0.268
Amlexanox	1856 ± 378	1878 ± 189	> 100
Neomycin	1021 ± 86	No binding	> 100
Ellipticine	1425 ± 138	1125 ± 201	1.117 ± 0.158
Amoxapine	No binding	No bindng	> 100
Compd 2	No binding	No binding	> 100
Tag1	1032 ± 52	1258 ± 324	> 100
Tag2	932 ± 26	955 ± 28	> 100
Tag3	1122 ± 254	1355 ± 168	0.175 ± 0.026
Tag4	1512 ± 46	1855 ± 458	> 100
Tag5	1953 ± 82	1058 ± 387	1.690 ± 0.32
Tag6	1393 ± 14	1228 ± 369	0.119 ± 0.078
Tag7	1134 ± 140	1145 ± 147	> 100
Tag8	2164 ± 137	1955 ± 249	> 100

* All values are expressed as mean ± SD (n = 3).

Figure 1. Design and screening of bifunctional RNA-binding compounds (tags) to modulate siRNA hydrophobicity

(A) A digraph to show compounds' chemical structure and action mode on siRNA modulation. The potential siRNA-binding group R is listed in the gray box, and the corresponding bifunctional tag is marked in parentheses. (B) A table to summarize compounds' affinity to siRNA/dsDNA and cytotoxicity to ARPE-19 cells. (C) The response curves of biolayer interferometry (BLI) assay showing the association and dissociation kinetics of tag2 (concentration: 250, 500, 1,000, 2,000, and 4,000 nM) to the immobilized siRNA on sensors. (D) Evaluation of time dependence of siRNA tagging (tag2 concentration: 200 nM) by fluorescence polarization. (E) Gel retardation assay to show the difference in migration rates between free siRNA (FAM labeled) and tagged siRNA (unlabeled). The siRNA for tagging is not labeled by FAM dye because it can be fluorescent (green) once intercalated with tag2. (F) Redistribution of siRNA from the water phase to the octanol phase with increase of tagging ratios. The red color indicates the fluorescence signal from sulfo-Cy5-labeled siRNA (50 nM). NA, not available.

than the parent compound. Nevertheless, quinacrine and the corresponding tag2 were finally selected as the lead for siRNA delivery due to their high affinity, low toxicity, and long history as safe drugs in antimalarial therapy.[23]

Despite affinity in the micromolar range (Figure 1C), BLI sensorgrams of tag2 demonstrate a fast association and dissociation kinetics to siRNA (K_{on} = 1.612 × 10^3 $M^{-1}s^{-1}$; K_{off} = 1.503 × 10^{-3} s^{-1}), indicating a fast tagging and detagging process. To further explore the binding kinetics, we examined the impact of incubation time on tagging efficiency using a fluorescence polarization assay (Figure 1D). The experiment was designed on the phenomenon that quinacrine can emit green fluorescence when it intercalates siRNA (Figure S3). By monitoring the polarized emission fluorescence signal, we found that elongation of incubation time can produce a higher order of tagging siRNA, suggestive of a time dependence in tagging. Meanwhile, a slight increment of molecular weight after siRNA tagging, reflected by the slower migration rate, was observed in the gel retardation assay (Figure 1E). The most exciting observation is the redistribution of siRNA from the water phase to the octanol phase with the increase of tagging ratios (Figure 1F, and its colored images are available in Figure S4). By comparing siRNA concentrations in two phases, we were able to calculate the partition coefficient (P) and logP value. At the highest tagging ratio

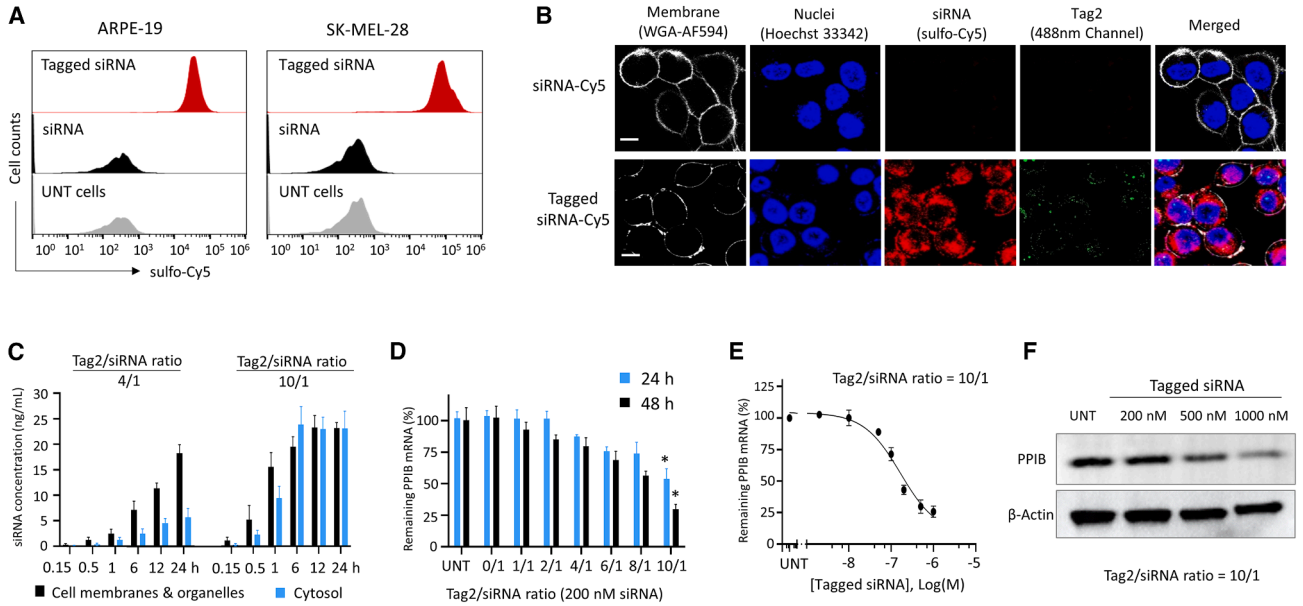

Figure 2. Cellular uptake, intracellular distribution, and RNAi activity of the hydrophobic tagged siRNA

(A) Enhanced uptake by ARPE-19 and SK-MEL-28 cells after siRNA tagging at a tag2/siRNA ratio of 10/1 (200 nM). (B) Confocal images to show the intracellular distribution of siRNAs (200 nM) with or without tagging. Cell line, ARPE-19. Scale bar, 10 μm. (C) Stemloop RT-qPCR to quantify the siRNA distribution in subcellular fractions at tagging ratios 4/1 and 10/1. (D) Gene silencing activity of the tagged anti-PPIB siRNA (200 nM) varies with the tagging ratio and treatment time. RNAi activity after 24- and 48-h treatment was measured in ARPE-19 cells. UNT, untreated cells. *$p < 0.05$. (E) Dose response of anti-PPIB siRNA tagged at a ratio 10/1 in ARPE-19 cells and measured at 48 h after treatment. The tagged siRNA has a RNAi IC_{50} of 166 ± 59 nM. (F) PPIB protein knockdown by the tagged siRNA in ARPE-19 cells at four concentrations.

(10/1), the logP value of siRNA is 1.86. This value is close to the ideal 1.35–1.8 for good oral absorption and permeation according to Lipinski's rule of 5.[26] Altogether, our data demonstrated the feasibility of siRNA transition from hydrophilicity to hydrophobicity by the small-molecule tagging method.

Compound-tagged siRNA is membrane permeable and self-deliverable

The successful modulation of siRNA hydrophobicity encouraged us to investigate whether the tagged siRNA is membrane permeable and self-deliverable. We first evaluated the free uptake of tagged siRNA (10/1) in ARPE-19 and SK-MEL-28 cells by flow cytometry, as shown in Figure 2A. These two cell lines were selected because they represent types of retinal cells and siRNA-easy-transfect cell lines, respectively. After 1-h incubation at 37°C, the tagged siRNA (sulfo-Cy5 labeled) can passively diffuse into cells by a concentration gradient at 200 nM, showing a remarkable right shift of mean fluorescent intensity compared with the naked siRNA. A similar uptake tendency was also observed by MDA-MB-231 and HeLa cells (Figure S5). To better visualize membrane permeation, uptake of the tagged siRNA was imaged by confocal microscopy on ARPE-19 (Figure 2B), MDA-MB-231, and SK-MEL-28 cells (Figure S6). Due to the relatively even modulation of cholesterol on the siRNA surface, we observed a strong deposition of siRNA in cytosol and the vesicular compartment, but not an association with plasma membrane (it was commonly seen in the uptake driven by cholesterol-siRNA conjugates).[18] By colocalization of the red fluorescence channel (sulfo-Cy5 on siRNA) and green channel (tag2), it was found that the tagged siRNA might have already dissociated after uptake. We speculated that the weak interaction between siRNA and tag2 was unable to hold these two physiochemically distinct components together in the context of a complicated intracellular environment. Instead, the hydrophilic siRNA tends to slip into the cytosol for better solubility, whereas the tag2 molecule may remain in the lipid bilayer due to its lipoid nature. Unfortunately, we were unable to trace the trafficking of tag2 in cells at the current stage, because tag2, once dissociated from siRNA, only emits a very weak green fluorescent signal. Confocal images might be unable to show its distribution inside cells. To better illustrate the distribution of siRNA inside cells, we tried to quantify the siRNA content in the subcellular fractions by stemloop RT-qPCR (Figure 2C). A close monitoring of siRNA distribution over time revealed that around half of the amount (50%) of siRNA can relocate into the cytosol at a high tagging ratio (tag2/siRNA ratio = 10) after 6 h, but the percentage reduces to ∼25% when the tagging ratio is set at 4/1, indicating the importance of the tagging ratio in siRNA delivery. Meanwhile, the cytosolic delivery of tagged siRNA (ratio 10/1) seems saturable after 6 h. The reason is unknown, but it is likely linked to the saturation of tag2 in the plasma membrane and corresponding defluidization,[27] as the less-tagged siRNA (ratio 4/1) can continue to enter cells even after 24 h.

Next, we studied the gene-silencing effect of the tagged anti-PPIB siRNA across different tag2/siRNA ratios. PPIB (peptidylprolyl isomerase B) is a housekeeping gene expressed in most mammalian

cells. A potent and fully modified siRNA sequence has been disclosed by Genentech.[28] Here, we used it as a model siRNA for our concept demonstration. As shown in Figure 2D, the RNAi effect is time related and tagging ratio dependent. The maximal effect was observed at the highest tagging ratio (10/1) and after 48-h treatment. Within the optimized condition, we plotted the dose-response curve of a tagged anti-PPIB siRNA on SK-MEL-28 cells (Figure 2E). By free uptake, the tagged siRNA shows an IC_{50} value at around 166 nM, and a maximum of 75% reduction in PPIB mRNA expression could be achieved. In comparison, it has been well documented that the cholesterol-siRNA conjugate is only able to knock down gene expression by ∼30% at a similar siRNA concentration.[29,30] The RNAi result was further confirmed by western blotting analysis of the downregulated PPIB protein (Figure 2F).

Screening and modification of miniature anti-VEGF siRNAs

Another factor that might affect the RNAi activity of tagged siRNA is the siRNA duplex structure. More specifically, the tagging system might prefer a miniature siRNA scaffold to promote permeation and penetration. The naturally occurring siRNA has a 19-bp duplex backbone and a 2-nt overhang at each end (19 + 2nt). Its large size, featured by over 13 kDa in molecular weight, 42 nt, and 42 anions, could be a huge burden to the tagging molecules during delivery. Besides the canonical structure, many siRNA designs have been reported to show negligible impact on the gene silencing activity. We were particularly interested in the asymmetric shorter-duplex siRNA structure 16 + 3A, which is truncated (only 35 nt) but efficiently triggers gene silencing in human cell lines.[31] We compared the RNAi activity of this scaffold (16 + 3A) with canonical siRNA and found that they are equally effective in our test (Figure S7). In this regard, we next tried to screen anti-VEGF siRNAs based on the 16 + 3A scaffold for ocular delivery.

To obtain a siRNA candidate, we designed and synthesized a panel of siRNAs targeting 44 sites (16 + 3A scaffold, Table S1) in the ORFs of human VEGF165 mRNA (VEGF 165 is the most abundant splice variant of VEGF-A gene). The screening system was established using a reporter construct, wherein the VEGF165 gene is positioned after the 3′ UTR of Renilla luciferase (Rluc). The reporter vector and siRNA library were co-transfected into HEK293T cells using the jetPRIME transfection reagent. The RNAi potency of individual siRNA at 1 and 0.1 nM was quantified after normalization to the internal firefly luciferase (Fluc) control. As shown in Figure 3A, several siRNA sequences showed a picomolar potency in the *in vitro* reporter assay. The three most potent candidates from the initial screen underwent further characterization in the VEGF-positive ARPE-19 cells using the standard real-time RT-qPCR assay (Figure S8). The result correlated well with the reporter assay, with the exception of si149. It outperformed the best candidate (si382) of the screen and elicited the most potent activity, suggestive of its better compatibility with the native context of the target mRNA.

Subsequent optimization focused on the chemical modification of si149 to increase its stability and immune safety. The most common modification in clinical siRNAs is the substitution of ribose 2′-OH using 2′-methoxy (2′-OMe) or 2′-fluoro (2′-F), and phosphoester bond (P=O) using phosphorothioate (P=S). These modifications can be arranged along with siRNA duplex sequence to form very diverse combinations but only a few patterns known to negligibly impact siRNA activity, including the enhanced stabilization chemistry (ESC) mode,[32] advanced ESC (adv ESC),[33] alternating 2′-OMe/F (alt OMe/F),[34] 2′-OMe U and C bases (UC OMe),[35] 2′-fluoro U and C bases (UC 2′-F),[36,37] etc. Here, we modified the 16-nt sense and 19-nt antisense strands separately using these chemistry modes, and then annealed them in a random order to obtain a total of 27 si149 duplexes, as shown in Figure 3B. By measuring the RNAi activity across all these duplexes via the RNAiMAX transfection, we found that most chemotypes did not work well with this 16 + 3A scaffold. Systematic analysis of data in Figure 3C revealed that the RNAi activity of miniature siRNAs was more sensitive to the chemotype of the antisense strand than the sense strand. For example, potent RNAi activity was only observed in the si149 siRNAs with antisense strand of UC 2′-F mode, whereas the sense strand could be any chemotypes. Because all the chemotypes we tested are known to well fit the RNA-induced silencing complex (RISC) processing, the interesting observation here might indicate that 16 + 3A duplexes of some chemotypes cannot form a classic configuration for RISC loading, especially in the 3-nt overhang region.[38] The conservative modes, such UC 2′-F and alt OMe/F, could be favored by a 16 + 3A scaffold. Because the UC 2′-F mode has a relatively low level of modification intensity, it raises worries about siRNA stability *in vivo*. As a compromise, we selected the sense strand of the adv ESC mode to duplex with it for a better stability, namely the siRNA candidate si149m13. It was tagged by siRNA-binding molecules tag2 and delivered into ARPE-19 cells to evaluate the duration of its RNAi activity. As shown in Figure 3D, siRNA si149m13 exhibits a slightly better effect than its unmodified parent, but not prominently. Due to the complexity of siRNA chemistry, further optimization was not pursued in this study.

Ocular delivery of the tagged siRNA to mouse retina

Ocular delivery was designed to determine whether the tagged siRNA was able to reduce the VEGF mRNA expression in the mouse retina after intravitreal injection (Figure 4A). The vitreous body is a relatively enclosed compartment, but intravitreal drugs can be eliminated via the anterior or posterior routes, i.e., across the blood-retina barriers to the systemic blood circulation.[39] To investigate the ocular pharmacokinetics, sulfo-Cy5.5-labeled siRNA was injected into the mouse vitreous body with or without tagging, and the drug remaining in the eyes was imaged using the Odyssey near-infrared fluorescent scanner. As shown in Figure 4B, the tagged siRNA showed a similar elimination profile to the naked siRNA, although the former is much more hydrophobic than the latter. Quantification of fluorescence intensity in eyeballs revealed that siRNAs have an ocular half-life of ∼24 h (Figure S9), which is longer than the small-molecule drugs but shorter than anti-VEGF antibodies.[40] This result was in agreement with the decay of siRNA fluorescence in living mouse eyes over time (Figure 4C). To illustrate the

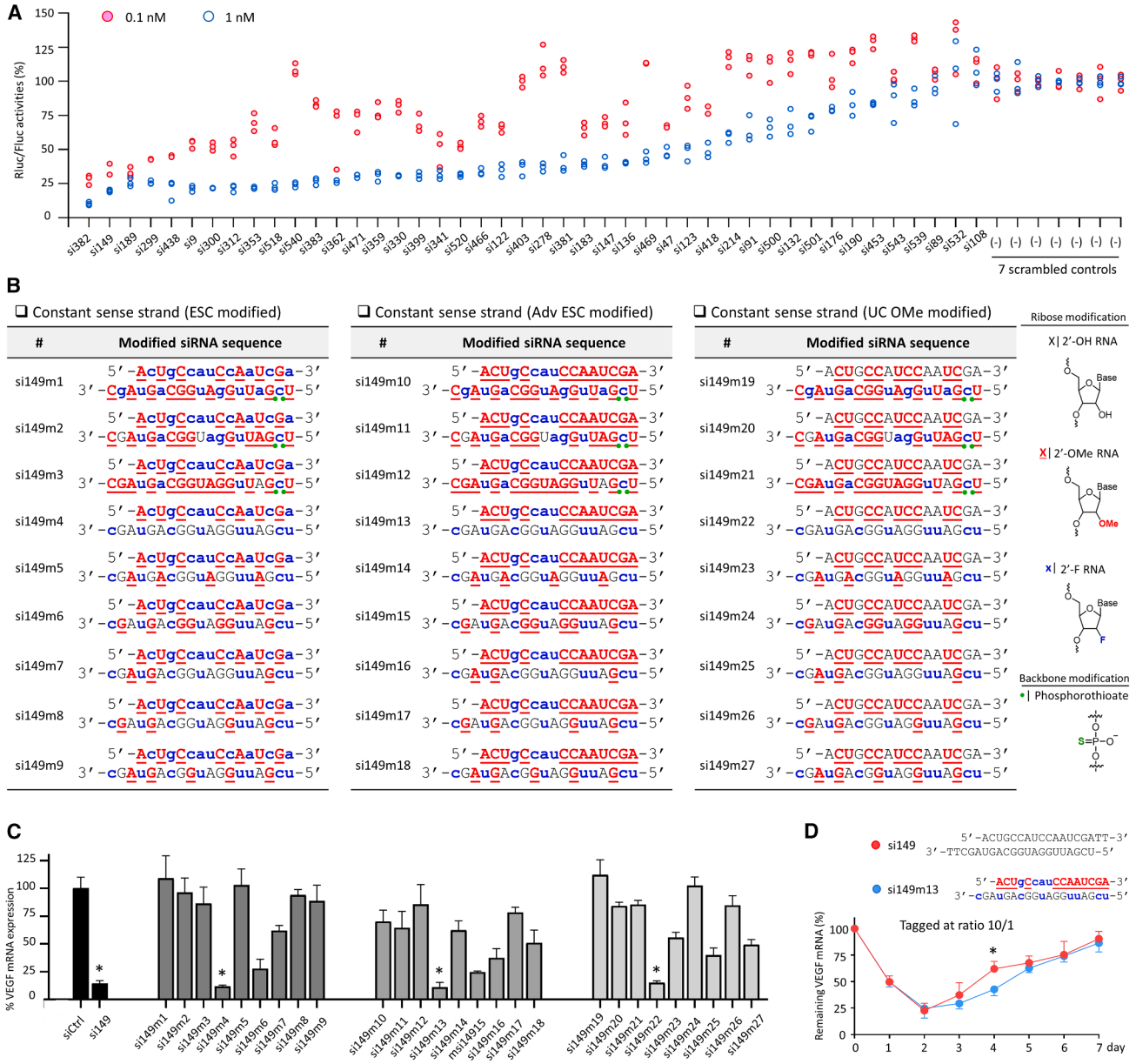

Figure 3. Identification of a miniature anti-VEGF siRNA with appropriate chemical modification

(A) Anti-VEGF siRNA screen in HEK293T reporter cells by the jetPRIME-mediated DNA/siRNA cotransfection. siRNA candidates were tested in triplicate at concentrations of 1 and 0.1 nM, respectively. (B) Tables to list si149 siRNA sequences with different modification chemotypes. (C) Real-time RT-qPCR assay to compare RNAi potency of chemically modified si149 siRNAs (10 nM) in ARPE-19 cells by RNAiMAX transfection. *$p < 0.01$. (D) Time course RNAi efficacy of si149 and si149m13 (500 nM) delivered by tag2 in ARPE-19 cells. *$p < 0.05$.

clearance pathway of tagged siRNA after intravitreal injection, we closely monitored the elimination kinetics of siRNA in mice eyes and other organs using the stemloop RT-qPCR quantification. The result in Figure 4D revealed that siRNA was only detectable in the eyes, kidney, and blood, indicating the possibility of a renal clearance pathway. It was reported that the hydrophobic siRNA could hijack the lipid transport pathway and accumulate in the liver[41]; whereas we did not observe the hepatic siRNA accumulation in our assay. We may envision that the siRNA has already dissociated from the tag when it passes through the blood-retina barriers and enters the systemic circulation.

As a local delivery strategy, intravitreal injection can apply high concentrations of tagged siRNA in the vitreous humor and drive its

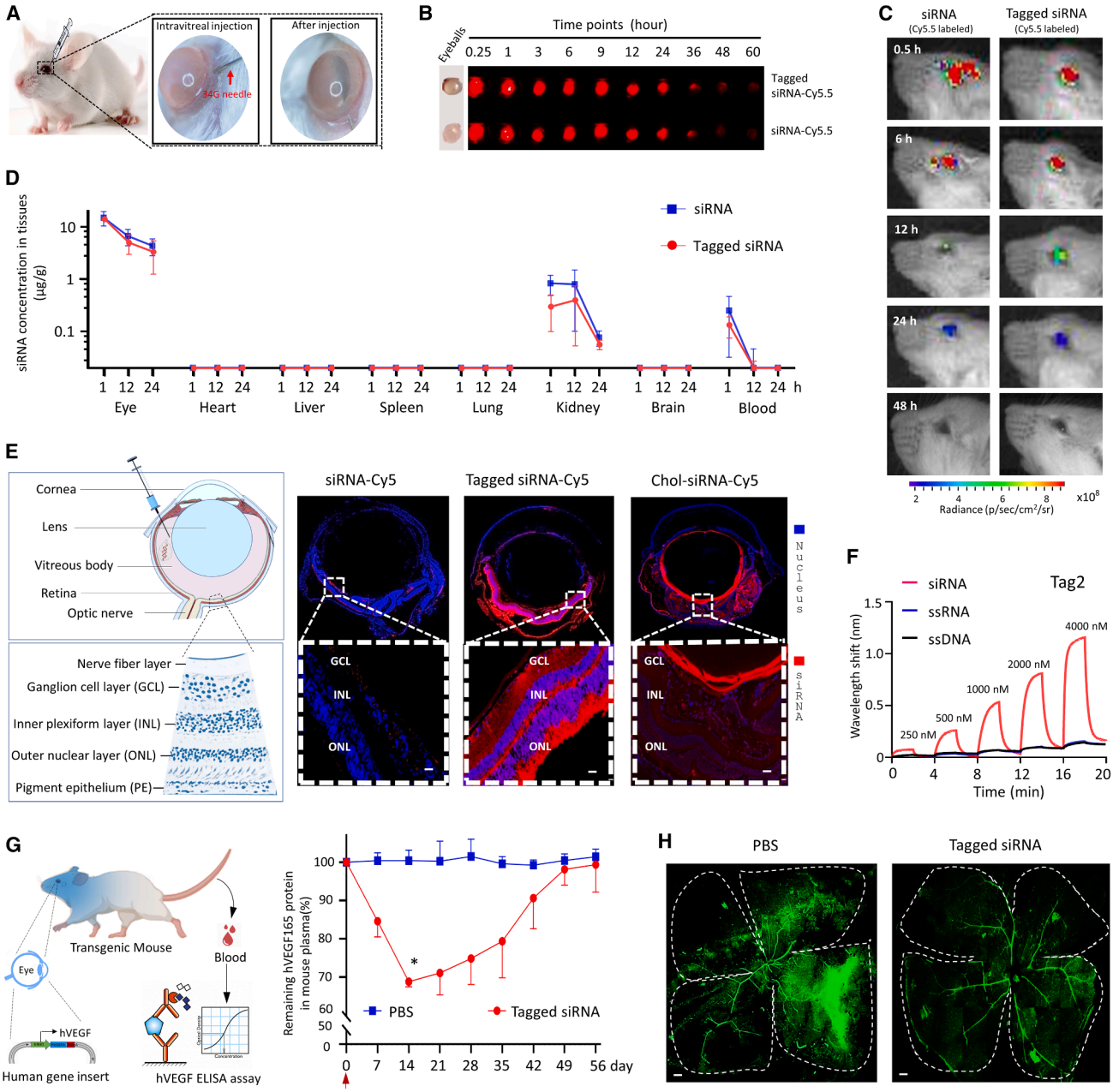

Figure 4. Ocular delivery of the tagged siRNA (si149m13) to retina by intravitreal injection in mice

(A) A demonstration of injection procedures under magnification from a Zeiss operating microscope. (B) Odyssey scanning of mouse eyeballs to compare the ocular retention of naked siRNA and tagged siRNA (11 ng). Both siRNAs were labeled by sulfo-Cy5.5 for near-infrared visualization. (C) *In vivo* tracing of sulfo-Cy5.5-labeled siRNA in mouse eyes over time after intravitreal injection (11 ng). (D) Quantification of siRNA concentrations in organs at 1, 12, and 24 h after intravitreal injection. (E) Retinal cross-sections of mice 12 h post injection of 1 μL siRNA (11 ng). siRNA distribution is seen through the fluorescence of the attached sulfo-Cy5 fluorophore. An anatomy of mouse eye and retinal layers is shown on the left. Scale bar, 10 μm. (F) The responses of tag2 to the double-stranded or single-stranded oligonucleotides (immobilized) in a BLI step-binding assay. (G) hVEGF protein knockdown as a function of time after a single intravitreal injection of tagged si149m13 (1.1 μg) in transgenic mice (n = 3 males per group). Ocular hVEGF level can be obtained by measuring protein concentration in mouse tail-vein blood via ELISA because of the connection between ocular and systemic circulations. The red arrow indicates the injection time. *$p < 0.05$. (H) Representative images of retinal flat mounts stained with lectin B4-AF488 to visualize vasculature after 30-day treatment by tagged si149m13 (1.1 μg). Scale bar, 100 μm.

diffusion into the retina layers by a passive concentration gradient. The mouse retina is composed of organized layers of nerve fibers, ganglion cells (GCL), inner plexiform (INL), outer nuclear (ONL), and pigment epithelium (PE), which has a global thickness of about 0.2 mm (Figure 4E).[42] To understand whether the tagged siRNA could diffuse into retinal layers following intravitreal injection, sulfo-Cy5-labeled siRNA (1 μL) was injected to allow penetration for 12 h, and the ocular frozen section was imaged to analyze the siRNA distribution in the retina. As shown in Figure 4E, the tagged siRNA achieved a nearly homogeneous distribution in the whole retina. The high deposition of siRNA-Cy5 could be seen even in the outermost PE layer that produces VEGF. On the contrary, cholesterol-siRNA conjugate can only penetrate the top layer, likely owing to its amphiphilic structure. There was staining of some ganglion cells by the naked siRNA (siRNA-Cy5) group, but it was weak and unevenly distributed. These results demonstrated that hydrophobicity modulation by tag2 enables siRNA to rapidly access all layers of the retina after intravitreal injection, suggestive of the feasibility to block all VEGF-expressing cells in eyes by RNAi therapy. It is worth noting that the tagging approach might not be applicable to the gapmer, phosphorodiamidate morpholino oligonucleotides, and other antisense oligonucleotides (ASOs), albeit their similar building blocks to siRNA. As shown in Figure 4F, the tag2 molecule exhibited a much stronger affinity to siRNA than the single-stranded oligonucleotide (ssRNA or ssDNA), likely owing to the binding bias to double strands by the intercalation mode. Other strategies, such as chemical modification by dendrimers and cell penetrating peptides, have been reported to facilitate the penetration of ASOs across retinal layers.[43,44]

In a transgenic mouse model with mild retinal neovascularization, we evaluated the VEGF suppression effect by the tagged siRNA. The retina of transgenic mice contains a human VEGFA (hVEGFA) gene driven by a truncated mouse rhodopsin promoter.[45] Ocular expression of hVEGF induces angiogenesis, focal leakage, microaneurysms, and other clinical changes associated with retinal diseases. Moreover, the key biomarker protein hVEGF165 could leak into the systemic circulation and be detected by the routine enzyme-linked immunosorbent assay (ELISA) method (Figure 4G). After intravitreal administration of the tagged siRNA, we closely monitored the fluctuation of hVEGF165 levels in mouse plasma. As shown in Figure 4G, a significant reduction of hVEGF165 expression was observed, and the suppression could last for 1.5 months. The duration of the RNAi effect was much shorter than the clinical siRNAs, but it could be explained by the suboptimal chemistry of our 16 + 3A siRNA (a low stability and lack of Ikaria modification). Nevertheless, retinal vascular permeability could be suppressed by a single dose of tagged siRNA (Figure 4H). These data suggested that siRNA tagged by bifunctional compounds can penetrate deeply and induce effective gene silencing in the retina.

DISCUSSION

Hydrophobicity is an important physicochemical property of drugs that correlates with their pharmaceutical behavior *in vivo*. It is often described by the parameter logP to help measure the drug likeness in drug discovery.[46] As a promising new modality, siRNA holds the extremely hydrophilic property, which prevents it from passive diffusion, membrane permeation, albumin hijacking, and uptake *in vivo*.[47] Hydrophobic modification, for example siRNA conjugation with lipids, is a popular strategy to overcome hydrophilicity and facilitate siRNA delivery.[16] Cholesterol- or fatty acid-siRNA conjugates have been reported to support extrahepatic delivery, but the tissue distribution and penetration is limited around the injection site, therefore considered as a local delivery strategy in many cases.[48] Cholesterol is highly hydrophobic, but its mini size is unable to cover the entire surface area of siRNA (6,619 $Å^2$), rendering the cholesterol-siRNA conjugate an amphiphilic rather than fully hydrophobic structure. Tethering multiple cholesterols at varying positions of siRNA strands is a chemically applicable approach, but extensive modification could seriously attenuate siRNA potency, despite some positive reports published.[49,50]

RNA-binding small molecules offer a means to manipulate siRNA hydrophobicity by the noncovalent approach.[51] In this study, we identified a siRNA-binding small-molecule quinacrine and functionalized it with cholesterol to generate a bifunctional tag for hydrophobic manipulation. Quinacrine interacts with the siRNA duplex via π-π stacking-based intercalation. A 19 bp siRNA could provide at least 6 binding sites for quinacrines by this action mode, thus allowing hydrophobic modulation extensively and evenly along with the siRNA chains.[52] Different from the amphiphilic cholesterol-siRNA conjugate, the tagged siRNA has a logP value of ∼2 and enables to distribute nearly completely in organic phase (octanol). The hydrophobicity enables the tagged siRNA not only to passively permeate the plasma membrane but also deeply penetrate mouse retinal layers and achieve an effective gene-silencing effect *in vivo*.

Notably, siRNA delivery by small-molecule tags could circumvent the endosomal entrapment. This was evidenced by a high portion (∼50%) of siRNA translocated to the cytosol in the subcellular fractionation assay. This percentage is much higher than that achieved by lipid nanoparticle (LNP) and GalNAc-siRNA (1%–2%).[53,54] However, it is common in delivery systems that rely on hydrophobic surfaces to passively penetrate cell membranes. Many cargos, including proteins and nanoparticles, have been reported to cross the plasma membrane and enter the cytosol effectively by either covalently or noncovalently tagging hydrophobic molecules.[55–59] It is worth noting that this approach generally requires a high-concentration gradient to drive the diffusion of cargos through the lipid bilayer, which is a shortcoming compared with the LNP and GalNAc technology.

Interestingly, siRNA partition between the cytosol and cellular membranes/organelles is heavily influenced by the siRNA/tag ratios. This observation might indicate a divergence of uptake mechanism at high and low ratios. We speculated that siRNA at a low tagging ratio was not fully covered by cholesterol, thus presenting an amphiphilic structure and tending to enter cells via endocytosis and the endosomal pathway. At the high ratio, the tagged siRNA is membrane compatible and able to reach the cytosol via passive diffusion.

Surprisingly, despite the efficient cytosolic delivery, the tagged siRNA did not produce a highly potent RNAi activity (IC_{50} = 166 nM) as expected. The reason is unknown, but it might be attributed to the inhibitory effect of the tag itself. More studies are encouraged to clarify the mechanism and improve the potency.

Both the naked siRNA and tagged siRNA have a half-life of around 24 h in the mouse eyes. This value is slightly shorter than the elimination half-lives of anti-VEGF antibodies in the mouse vitreous ($t_{1/2}$ 27 h).[60] However, intravitreal pharmacokinetics is usually studied in rabbits, because they have much larger humor volumes than mice (1,500 vs. 5 μL) and thus enable pharmacokinetic translation to man.[61] A study reported that the half-life of chemically modified siRNA in the vitreous of the Dutch Belted rabbit could be about 2 days.[62] We may estimate an ocular half-life of around 3 days in humans according to the rabbit-to-man scaling factor of 1.4 from the report of Del Amo et al.[63] Moreover, the penetration in the retina is driven by the concentration gradient of tagged siRNA. The long half-life can provide a constant high concentration and strong driving force to penetrate deeper into the human retina. The tagged siRNA seems able to penetrate deeper than the thickness of mouse retinal layers because there is no fluorescence intensity gradient in retinal cross-section images. Moreover, we have noticed the presence of a siRNA-Cy5 signal in the inferior oblique muscle. Since this tissue is located outside the retina and sclera layers, we may speculate that the tagged siRNA could go beyond the retinal layer of mice. This result also indicates that siRNA remains tagged when it interacts with the retina and passes through cell layers. Therefore, the tag dissociation process (detagging) in cytosols is likely slower than the transcytosis speed, otherwise the siRNA would be detagged and trapped in the cytosol of first-layer cells during transcytosis. Because the tag2 itself has only a very faint fluorescence signal, it is hard to trace the detagging event in cells (even *in vitro*) by confocal imaging experiments. A follow-up study by dedicated design is on the way to clarify the penetration-detagging relationship.

In sum, we reveal a new RNA-binding bifunctional compound that can bind siRNA and modulate its hydrophobicity. The key component, a siRNA-binding group, was screened and identified from 12 siRNA intercalators. The candidate quinacrine features a good affinity and biosafety. The quinacrine-based bifunctional compound can tag around the siRNA backbone and transform it into a hydrophobic, membrane-permeable, and self-deliverable form. Moreover, ocular delivery of an anti-VEGF miniature siRNA by the compound can penetrate deeply into mouse retinal layers and induce effective gene silencing, showing potentials to treat retinal diseases.

MATERIALS AND METHODS

Test compounds

The compounds used in the *in vitro* experiments were obtained from Bide Pharmatech (Shanghai, China). According to the suppliers, all compounds had purities of at least 95%, as verified by high-performance liquid chromatography (HPLC) analysis. All the tags were synthesized and analyzed according the procedures in the supplemental information. The tag compounds were 95% pure by HPLC analysis.

BLI test

The AR2G amine coupling biosensor was activated by EDCI and NHS solution at pH 5.0, followed by immobilization of amino siRNA (3′ terminus of sense strand) or DNA onto sensor tips. After reaction, remaining active sites on sensors were blocked with ethanolamine solution at pH 8.5. A serial concentration of test compounds (250, 500, 1,000, 2,000, and 4,000 nM) was loaded into corresponding wells of a black 96-well plate, followed by sequentially undergoing baseline, association, dissociation, and regeneration cycles on sensors. Data analysis was performed using Data Analysis 11.1 for curve fitting and GraphPad Prism for graphical presentation. Sequences of siRNA and dsDNA are as follow:

siRNA sense (siPPIB): A$\underline{C}$A$\underline{G}$C$\underline{A}$A$\underline{A}$U$\underline{U}$C$\underline{C}$A$\underline{U}$C$\underline{G}$U$\underline{G}$U*T*T-C6-NH_2; siRNA antisense (siPPIB): $\underline{A}$C$\underline{A}$C$\underline{G}$A$\underline{U}$G$\underline{G}$A$\underline{A}$U$\underline{U}$U$\underline{G}$C$\underline{U}$G$\underline{U}$* T*T.; DNA sense: AGGGCAGAATCATCACGAAGTGGT-C6-NH_2; DNA antisense: ACCACTTCGTGATGATTCTGCCCT.

In the above sequences, the 2′-OMe ribosugar and P=S linkage modification are represented by the underline and *, respectively. The sense strand 3′ terminus was modified by a hexylamine (C6-NH_2) group for sensor immobilization.

Cytotoxicity test

The viability of ARPE-19 after different compound treatment was measured using the Cell Counting Kit-8 (CCK-8) assay. Briefly, ARPE-19 (5,000 cells/well, 5 repeat wells) was seeded in 96-well plates and allowed to attach for 24 h. A series of compound concentrations (10^{-1}–10^{6} nM) was applied and co-incubated with cells for 48 h. The viable cells were analyzed using the CCK-8 kit according to the manufacturer's protocol. The cell viability was expressed as a percentage relative to the value of untreated controls (100%).

siRNA tagging

To tag siRNA, the tag2 compound was first homogenously dispersed in PBS buffer (pH 7.4) through ultrasonic processing for 5 min in an ultrasonic water bath (Doves ultrasonic cleaner, 3.2 L, 180 W). The stock solution of tag2 (200 μM) was then combined with siRNA at predetermined stoichiometric ratios in microcentrifuge tubes. The reaction mixture was subjected to incubation at 37°C for 12 h, with occasional agitation to ensure uniform mixture.

Fluorescence polarization

Fluorescence polarization assays were used to determine the association between tag2 and siRNA. The experimental parameters were set up according to Wang's report.[64] Briefly, tag2 was titrated to obtain an optimal concentration (200 nM) for fluorescence polarization assay (Figure S10). Then experiments were performed in black flat-bottom 96-well plates at a final volume of 100 μL. After tagging, the plate was incubated for 2 or 12 h at 37°C before the

measurement. The polarization signal was read by a microplate reader (Tecan SPARK) at λ_{ex} = 450 nm, λ_{em} = 530 nm.

Gel retardation assay

Agarose (0.5 g) was weighed and placed in a conical flask, followed by addition of 50 mL of 1× TBE buffer. The agarose solution was heated using a microwave oven until complete dissolved. The gel solution was molded into a 1% agarose gel without adding any staining agent. siRNA (1 μL, 10 μM stock solution) was tagged by tag2 at different ratios, then loaded into the wells. The samples were electrophoresed at 100 V and run for 10 min before imaging. FAM-labeled siRNA (siRNA-FAM) was used as a control to show the migration of free siRNA.

LogP assessment

The sulfo-Cy5-labeled siRNA (siRNA-Cy5) was dissolved in the aqueous phase to a final concentration of 50 nM, while the compound tag2 was dissolved in n-octanol at the required experimental ratio (1/1–10/1). Equal volumes (0.2 mL each) of the two-phase solutions were placed in a test tube, and the mixture was thoroughly shaken at 25°C to reach equilibrium distribution. After allowing the mixture to stand for 12 h, the siRNA partition in the two phases was imaged using the Odyssey CLx Imaging System (LI-COR Biosciences). To obtain the logP values, the siRNA concentrations in the two phases (C_o and C_w) were quantified by measuring the Cy5 fluorescence intensity. The partition coefficient was calculated using the formula $P = C_o/C_w$. The logP value was obtained by taking the logarithm of the distribution coefficient.

Cell culture

Roswell Park Memorial Institute (RPMI) 1640 medium, fetal bovine serum, and other cell culture supplementary reagents were purchased from Procell (Wuhan, China). SK-MEL-28, ARPE-19, HeLa, and HEK293T cells were obtained from the American Type Culture Collection and cultured in RPMI 1640 medium supplemented with 10% fetal bovine serum, 100 μg/mL streptomycin, and 100 U/mL penicillin. The cells were maintained at 37°C in a humidified atmosphere of 5% CO_2.

Flow cytometry

Flow cytometry was used to analyze the cellular uptake of tagged siRNA. Briefly, 10,000 cells were suspended in serum-free RPMI 1640 medium. After incubation with siRNA (200 nM) for 1 h at 37°C, cells were spun down, washed twice with PBS buffer, and resuspended in RPMI 1640. Cells were kept on ice until flow cytometry analysis. The analysis was performed using a Beckman Coulter CytoFLEX S instrument, and data were processed using FlowJo software.

Confocal imaging

To trace the distribution of tagged siRNA inside cells (ARPE-19, SK-MEL-28, and MDA-MB-231), sulfo-Cy5-labeled siRNA (tagged or untagged, 200 nM) was incubated with cells in the serum-free RPMI 1640 medium for 6 h. The cell monolayer was washed and imaged using a Leica Stellaris 5 WLL confocal microscope equipped with a HyD detector and excitation lasers at 405, 488, 561, and 640 nm. The nuclei and cell membranes were counterstained with Hoechst 33342 and WGA-AF594, respectively. The excitation wavelength for detecting Tag2 was 488 nm.

siRNA quantification in subcellular fractions by stemloop RT-qPCR

To quantify siRNA in subcellular fractions, a stemloop RT-qPCR assay was developed according to reports.[65,66] Custom DNA forward primers, reverse primers, reverse transcription (RT) primers, and TaqMan probes were all obtained from Sangon Biotech (Shanghai, China). Their sequences are available in Table S2. In brief, cell monolayers in 24-well plate were treated with siRNA (200 nM) at 37°C for the indicated time intervals (0.15, 0.5, 1, 6, 12, and 24 h). Cells were washed, resuspended in 100 μL PBS buffer, and passed through narrow-gauge equipment several times to homogenize. The lysate was subjected to high-speed centrifugation (100,000 × *g* for 1 h) to carefully separate the supernatant (containing cytosolic siRNA) from the pellet (containing membrane and organelles). The pellet was resuspended in 100 μL PBS, heated (1 min at 95°C) and cooled to room temperature. One microliter of siRNA fraction solution (from supernation or pellet) was aliquoted for stemloop reverse transcription (MR101, Vazyme), followed by real-time qPCR quantification using the AceQ qPCR Probe Master Mix (Vazyme, Q112). The measured CT values were then applied to a standard curve to determine the corresponding siRNA concentrations.

Real-time RT-qPCR

The extraction of total cellular RNA from ARPE-19 was performed using the TRIzol Reagent (Vazyme, R411) according to the manufacturer's protocol. The extracted RNA was normalized to equal concentration and 5 μL was aliquoted for real-time qPCR assay using the HiScript II One Step SYBR Green Kit (Q221, Vazyme). RT-qPCR was performed on a Bio-Rad CFX Connect and analyzed using Bio-Rad CFX maestro software. Housekeeping gene β-actin was used as an internal control, and relative expression level of the genes was calculated by the $2^{-\Delta\Delta Ct}$ relative to the control group. Primer sequences: PPIB forward, 5′-GATGGCACAGGAGGAAAGAG-3′; PPIB reverse, 5′-AGCCAGGCTGTCTTGACTGT-3′; β-actin forward, 5′-TCCCATCACCATCTTCCA-3′; β-actin reverse, 5′-ATACTCCTGCTTGCTGATCC-3′; VEGF forward, 5′-AGGGCAGAATCATCACGAAGTGGT-3′; VEGF reverse, 5′-TCTGCATGGTGATGTTGGACTCCT-3′.

Western blotting

The cell sample was lysed using a cold IP lysis buffer supplemented with a protease inhibitor cocktail. After centrifugation at 4°C for 15 min (13,000 rpm), the supernatant of the cell lysate was collected and the protein concentrations were determined using a BCA Protein Assay kit (Thermo Fisher Scientific, 23227) according to the manufacturer's instruction. Twenty micrograms of total protein extracts was loaded in wells and electrophoresed on 12% SDS polyacrylamide gels, then transferred to 0.45 μm PVDF membranes. These membranes were blocked using TBST plus 1% BSA for 2 h

at room temperature. The membranes were subsequently incubated with the primary antibody (mouse anti-PPIB polyclonal antibody, Proteintech, 66047, dilution 1:3,000; mouse anti-β-actin monoclonal antibody, Abclonal, AC004, dilution 1:10,000) overnight at 4°C. Subsequently, goat anti-mouse secondary antibody coupled with horseradish peroxidase (Thermo Fisher Scientific, 31430; dilution 1:10,000) was applied at room temperature for 2 h. After three washes with TBST buffer, enhanced chemiluminescent horseradish peroxidase (HRP) substrate (Proteintech, PK10001) was added and chemiluminescence was detected using the ChemiDoc XRS+ Gel Imaging System (Bio-Rad).

Anti-VEGF siRNA screen using reporter cells and dual-luciferase reporter assay

The screen assay is designed by silencing the reporter gene encoded in plasmid psiCHECK-2/VEGF165. The reporter plasmid contains the cDNA encoding human VEGF165 gene (GenBank: AB021221.1), Renilla luciferase reporter gene and a separate firefly luciferase as a reference. To screen siRNA, siRNA and reporter plasmid were co-transfected to HEK293T cells using jetPRIME transfection reagent. Briefly, HEK293T cells were seeded in a 96-well plate at a density of approximately 10,000 cells per well. siRNA of different sequences was co-transfected at two concentration gradients (1 and 0.1 nM) along with 85 ng of psiCHECK-2/VEGF165 plasmid using 0.3 μL jetPRIME reagent per well. Twenty-four hours post transfection, the activities of firefly luciferase and Renilla luciferase were measured using the Dual Luciferase Reporter Gene Assay Kit (Vazyme, DL101). Reagents were added to the cell culture plate in volumes equal to the culture medium and incubated for 10 min. Chemiluminescence was detected using a multifunctional microplate reader (Tecan). Renilla luciferase served as an internal control, and the siRNA activity was calculated by dividing the Renilla luciferase RLU (relative light unit) value by the Firefly luciferase RLU value. The resulting ratio was used to evaluate the gene silencing efficiency of the reporter gene.

Intravitreal injection

All the animal studies were performed under the protocol approved by the Institutional Animal Care and Use Committee of Wuhan University, in accordance with the guidelines of the Chinese Regulations for the Administration of Affairs Concerning Experimental Animals. Intravitreal injections in mice were performed following a protocol from Cameron et al.[67] Briefly, 9-week-old Balb/c mice (Changsheng Biotech) or transgene mice strain B6-Rho-hVEGFA-Tg (Gempharmatech, T036939) were anesthetized by intraperitoneal administration of 0.1 mL of amobarbital (1%, w/v, in saline). Under an operating microscope, 1 μL of chol-siRNA, tagged siRNA or naked siRNA (1 or 100 μM) were intravitreally injected using a 2.5-μL Hamilton syringe equipped with a 34G needle. The needle was positioned 1 mm posterior to the limbus and 1 μL of the solution was slowly (3–5 s) injected into the vitreous chamber of the eye. A 30-s interval was kept before removing the needle. The left and right eyes of the mice were injected in parallel. After injection, sterile saline was used to rinse the eye.

Ocular pharmacokinetic study

To investigate the retention time of siRNA and tagged siRNA in the mouse vitreous, 1 μL of siRNA or tagged siRNA (1 μM, sulfo-Cy5.5 labeled) was injected into the vitreous body using a microinjector. At the designated time points (0.5, 6, 12, 24, and 48 h), mice were imaged using the IVIS *in vivo* imaging system (Bruker Xtreme BI). For *ex vivo* imaging, the mice were euthanized at the corresponding time points. The eyeballs were immediately enucleated and placed in PBS buffer for imaging analysis using the Odyssey infrared imaging system (LI-COR). The fluorescence intensity was quantified by Image Studio software and plotted against time to generate the ocular pharmacokinetics.

siRNA tissue distribution and quantification

After intravitreal injection of tagged siRNA or siRNA (1.1 μg), Balb/c mice were euthanized and dissected at 1, 12, and 24 h to collect tissue/blood samples. All samples, excluding blood, were snap-frozen in liquid nitrogen and ground into powder in a pre-cooled (4°C) tissue homogenizer (Servicebio) with 4-mm steel grinding balls at 30 cycles/s for 5 min. The powder was reconstituted at 100 mg/mL in PBS containing 0.25% Triton X-100 and resuspended using a tissue homogenizer. The homogenized samples were then heated at 95°C for 5 min, briefly vortexed, and allowed to rest on ice for 5 min. Subsequently, the samples were centrifuged at 10,000 × *g* for 5 min at 4°C. Whole blood (100 μL) was combined with an equal volume of PBS containing 0.25% Triton X-100 and homogenized at 4°C. The homogenate was heated at 95°C for 5 min, and centrifuged at 10,000 × *g* for 3 min at 4°C. The siRNA-containing supernatant was transferred to new tubes, and siRNA were quantified using the stemloop RT-qPCR method as described above.

Histology

Mouse eyeballs were collected 12 h post injection of sulfo-Cy5-labeled siRNA (11 ng) and fixed in 4% paraformaldehyde for 4 h. Tissue was embedded in OCT medium with care to avoid bubble formation, followed by storage at −80°C for cryopreservation. For sectioning, the tissue block was mounted on the cryostat with the freezing temperature precisely adjusted. Twenty minutes after temperature equilibration on the freezing stage, several sections were rapidly cut following the nasal-temporal direction of tissue, which allows sections containing the visual streak in the center of eyes to be collected. Sections with optimal morphological preservation were selected for slide mounting. Nuclei were counterstained with DAPI and siRNA was visualized by their sulfo-Cy5 signal. Histology images were collected using the 3DHISTECH CaseViewer Pannoramic scanner.

ELISA to analyze the VEGF165 protein level in blood

Fifty microliters of whole blood was sampled from the tail vein of transgenic mice (strain no. B6-Rho-hVEGFA-Tg, Gempharmatech) at the indicated days after intravitreal injection (1.1 μg). The blood was immediately diluted with 100 μL DPBS. After centrifugation at 1,200 × *g* for 10 min at 4°C, the supernatant was collected and stored at −80°C for subsequent use. According to the instruction

of the ELISA assay kit (Beyotime, PV963), samples and serial dilutions of the standard were loaded into wells precoated by anti-VEGF capture antibody. The wells were incubated at room temperature for 120 min. After washing five times by TBST, the biotinylated detection antibody was added and incubated for 60 min at room temperature. Wells were then washed and HRP-conjugated streptavidin applied for 30 min in the dark. After washing five times with TBST, TMB substrate solution was added and incubated for 30 min. The reaction was then stopped by 2N H_2SO_4 and absorbance at 450 nm was immediately measured by a microplate reader (Tecan).

Mouse retinal flat mount and fluorescence staining experiment

Flat mount dissection and staining were performed according to the protocol of Cameron et al.[67] Briefly, mice were anesthetized by intraperitoneal injection of pentobarbital, followed by transcardial perfusion with 50 mL saline. After perfusion, the eyeballs were enucleated and fixed in 4% paraformaldehyde at room temperature for 60 min. The retina was carefully extruded and four radial cuts centered on the optic disc were made to create a flat-mounting preparation. The retina was incubated in 0.3% Triton X-100 solution plus 1% BSA at room temperature for 12 h, followed by overnight incubation with Alexa fluor 488-conjugated *Griffonia simplicifolia* lectin I (GSL I-B4-Alexa fluor 488, Thermo Fisher Scientific, I21411) at room temperature. The retina was rinsed with sterile DPBS for 2 h, then carefully mounted onto a glass slide using antifade mounting medium and coverslip. Fluorescence images were acquired using a confocal microscope (Leica) at 488 nm excitation wavelength.

Statistical analysis

Statistical analysis was performed using GraphPad Prism 9.3.0, data are presented as mean ± standard deviation, p values were calculated using two-way ANOVA with Tukey's multiple comparison test, $p < 0.05$ was considered to be statistically significant.

DATA AND CODE AVAILABILITY

All the data and experimental parameters related to this paper are available in the main text and the materials and methods.

ACKNOWLEDGMENTS

This work was financially supported by the National Key R&D Program of China (grant no. 2021YFA0909900) and the National Natural Science Foundation of China (grant no. 82073770). The authors thank Prof. Rubi Mahato of Binghamton University for language/scientific assistance.

AUTHOR CONTRIBUTIONS

Q.M. and W.T. conceptualized and developed the project. Q.M., Y.Q., and S.C. performed the experiments and interpreted the data. Q.M. and W.T. wrote the manuscript.

DECLARATION OF INTERESTS

The authors declare no competing interests.

SUPPLEMENTAL INFORMATION

Supplemental information can be found online at https://doi.org/10.1016/j.omtn.2025.102751.

REFERENCES

1. Penn, J.S., Madan, A., Caldwell, R.B., Bartoli, M., Caldwell, R.W., and Hartnett, M.E. (2008). Vascular endothelial growth factor in eye disease. Prog. Retin. Eye Res. *27*, 331–371.
2. Spilsbury, K., Garrett, K.L., Shen, W.Y., Constable, I.J., and Rakoczy, P.E. (2000). Overexpression of vascular endothelial growth factor (VEGF) in the retinal pigment epithelium leads to the development of choroidal neovascularization. Am. J. Pathol. *157*, 135–144.
3. Ghanchi, F., Bourne, R., Downes, S.M., Gale, R., Rennie, C., Tapply, I., and Sivaprasad, S. (2022). An update on long-acting therapies in chronic sight-threatening eye diseases of the posterior segment: AMD, DMO, RVO, uveitis and glaucoma. Eye *36*, 1154–1167.
4. Gotadki, R. Anti-VEGF Market Research Report Information by Product (Eylea, Lucentis, and Beovu), by Disease (Macular Edema, Diabetic Retinopathy, Retinal Vein Occlusion, and Age-Related Macular Degeneration) and by Region (North America, Europe, Asia-Pacific, And Rest Of The World) – Industry Forecast Till 2034, 2025. Report MRFR/HC/20363-HCR.
5. Jakubiak, P., Alvarez-Sánchez, R., Fueth, M., Broders, O., Kettenberger, H., Stubenrauch, K., and Caruso, A. (2021). Ocular Pharmacokinetics of Intravitreally Injected Protein Therapeutics: Comparison among Standard-of-Care Formats. Mol. Pharm. *18*, 2208–2217.
6. Falavarjani, K.G., and Nguyen, Q.D. (2013). Adverse events and complications associated with intravitreal injection of anti-VEGF agents: a review of literature. Eye *27*, 787–794.
7. Lanzetta, P., Korobelnik, J.-F., Heier, J.S., Leal, S., Holz, F.G., Clark, W.L., Eichenbaum, D., Iida, T., Xiaodong, S., Berliner, A.J., et al. (2024). Intravitreal aflibercept 8 mg in neovascular age-related macular degeneration (PULSAR): 48-week results from a randomised, double-masked, non-inferiority, phase 3 trial. Lancet *403*, 1141–1152.
8. Adrianto, M.F., Annuryanti, F., Wilson, C.G., Sheshala, R., and Thakur, R.R.S. (2022). In vitro dissolution testing models of ocular implants for posterior segment drug delivery. Drug Deliv. Transl. Res. *12*, 1355–1375.
9. Guzman-Aranguez, A., Loma, P., and Pintor, J. (2013). Small-interfering RNAs (siRNAs) as a promising tool for ocular therapy. Br. J. Pharmacol. *170*, 730–747.
10. Khvorova, A. (2023). siRNAs—A New Class of Medicines. JAMA *329*, 2185–2186.
11. Murad, A., Lasko, M., Badri, P., Jadhav, S., Boyle, K., Li, J., Vest, J., and Taubel, J. (2024). A Phase 1, Single Ascending Dose Study to Evaluate ALN-TTRsc04, a Next-Generation RNA Interference Therapeutic, in Healthy Participants for Potential Treatment of Transthyretin Amyloidosis. Circulation *150*, A4135443.
12. Reich, S.J., Fosnot, J., Kuroki, A., Tang, W., Yang, X., Maguire, A.M., Bennett, J., and Tolentino, M.J. (2003). Small interfering RNA (siRNA) targeting VEGF effectively inhibits ocular neovascularization in a mouse model. Mol. Vis. *9*, 210–216.
13. Shen, J., Samul, R., Silva, R.L., Akiyama, H., Liu, H., Saishin, Y., Hackett, S.F., Zinnen, S., Kossen, K., Fosnaugh, K., et al. (2006). Suppression of ocular neovascularization with siRNA targeting VEGF receptor 1. Gene. Ther. *13*, 225–234.
14. Kaiser, P.K., Symons, R.C.A., Shah, S.M., Quinlan, E.J., Tabandeh, H., Do, D.V., Reisen, G., Lockridge, J.A., Short, B., Guerciolini, R., et al. (2010). RNAi-based treatment for neovascular age-related macular degeneration by Sirna-027. Am. J. Ophthalmol. *150*, 33–39.e2.
15. Garba, A.O., and Mousa, S.A. (2010). Bevasiranib for the treatment of wet, age-related macular degeneration. Ophthalmol. Eye Dis. *2*, 75–83.
16. Tai, W. (2019). Chemical modulation of siRNA lipophilicity for efficient delivery. J. Control. Release *307*, 98–107.
17. Petrova, N.S., Chernikov, I.V., Meschaninova, M.I., Dovydenko, I.S., Venyaminova, A.G., Zenkova, M.A., Vlassov, V.V., and Chernolovskaya, E.L. (2012). Carrier-free cellular uptake and the gene-silencing activity of the lipophilic siRNAs is strongly affected by the length of the linker between siRNA and lipophilic group. Nucleic Acids Res. *40*, 2330–2344.
18. Ly, S., Navaroli, D.M., Didiot, M.C., Cardia, J., Pandarinathan, L., Alterman, J.F., Fogarty, K., Standley, C., Lifshitz, L.M., Bellve, K.D., et al. (2017). Visualization of self-delivering hydrophobically modified siRNA cellular internalization. Nucleic Acids Res. *45*, 15–25.

19. Cheng, S.Y., Caiazzi, J., Biscans, A., Alterman, J.F., Echeverria, D., McHugh, N., Hassler, M., Jolly, S., Giguere, D., Cipi, J., et al. (2024). Single intravitreal administration of a tetravalent siRNA exhibits robust and efficient gene silencing in mouse and pig photoreceptors. Mol. Ther. Nucleic Acids *35*, 102088.

20. Byrne, M., Tzekov, R., Wang, Y., Rodgers, A., Cardia, J., Ford, G., Holton, K., Pandarinathan, L., Lapierre, J., Stanney, W., et al. (2013). Novel hydrophobically modified asymmetric RNAi compounds (sd-rxRNA) demonstrate robust efficacy in the eye. J. Ocul. Pharmacol. Ther. *29*, 855–864.

21. (2015). Update on phase 2 clinical trial results of RXI-109 treatment to reduce the formation of hypertrophic dermal scars. J. Am. Acad. Dermatol. *72*, AB273.

22. Tai, W., and Gao, X. (2018). Noncovalent tagging of siRNA with steroids for transmembrane delivery. Biomaterials *178*, 720–727.

23. Ehsanian, R., Van Waes, C., and Feller, S.M. (2011). Beyond DNA binding - a review of the potential mechanisms mediating quinacrine's therapeutic activities in parasitic infections, inflammation, and cancers. Cell Commun. Signal. *9*, 13.

24. Arya, D.P., Xue, L., and Willis, B. (2003). Aminoglycoside (neomycin) preference is for A-form nucleic acids, not just RNA: results from a competition dialysis study. J. Am. Chem. Soc. *125*, 10148–10149.

25. Nahar, S., Ranjan, N., Ray, A., Arya, D.P., and Maiti, S. (2015). Potent inhibition of miR-27a by neomycin-bisbenzimidazole conjugates. Chem. Sci. *6*, 5837–5846.

26. Shultz, M.D. (2019). Two Decades under the Influence of the Rule of Five and the Changing Properties of Approved Oral Drugs. J. Med. Chem. *62*, 1701–1714.

27. Ahmed, M. (2024). The Role of Cholesterol in Membrane Fluidity and Stability. J. Membr. Sci. Technol. *14*, 408.

28. Cuellar, T.L., Barnes, D., Nelson, C., Tanguay, J., Yu, S.F., Wen, X., Scales, S.J., Gesch, J., Davis, D., van Brabant Smith, A., et al. (2015). Systematic evaluation of antibody-mediated siRNA delivery using an industrial platform of THIOMAB-siRNA conjugates. Nucleic Acids Res. *43*, 1189–1203.

29. Gilleron, J., Paramasivam, P., Zeigerer, A., Querbes, W., Marsico, G., Andree, C., Seifert, S., Amaya, P., Stöter, M., Koteliansky, V., et al. (2015). Identification of siRNA delivery enhancers by a chemical library screen. Nucleic Acids Res. *43*, 7984–8001.

30. Ding, Y., Wang, W., Feng, M., Wang, Y., Zhou, J., Ding, X., Zhou, X., Liu, C., Wang, R., and Zhang, Q. (2012). A biomimetic nanovector-mediated targeted cholesterol-conjugated siRNA delivery for tumor gene therapy. Biomaterials *33*, 8893–8905.

31. Chang, C.I., Yoo, J.W., Hong, S.W., Lee, S.E., Kang, H.S., Sun, X., Rogoff, H.A., Ban, C., Kim, S., Li, C.J., and Lee, D.K. (2009). Asymmetric shorter-duplex siRNA structures trigger efficient gene silencing with reduced nonspecific effects. Mol. Ther. *17*, 725–732.

32. Nair, J.K., Willoughby, J.L.S., Chan, A., Charisse, K., Alam, M.R., Wang, Q., Hoekstra, M., Kandasamy, P., Kel'in, A.V., Milstein, S., et al. (2014). Multivalent N-Acetylgalactosamine-Conjugated siRNA Localizes in Hepatocytes and Elicits Robust RNAi-Mediated Gene Silencing. J. Am. Chem. Soc. *136*, 16958–16961.

33. Foster, D.J., Brown, C.R., Shaikh, S., Trapp, C., Schlegel, M.K., Qian, K., Sehgal, A., Rajeev, K.G., Jadhav, V., Manoharan, M., et al. (2018). Advanced siRNA Designs Further Improve In Vivo Performance of GalNAc-siRNA Conjugates. Mol. Ther. *26*, 708–717.

34. Allerson, C.R., Sioufi, N., Jarres, R., Prakash, T.P., Naik, N., Berdeja, A., Wanders, L., Griffey, R.H., Swayze, E.E., and Bhat, B. (2005). Fully 2'-modified oligonucleotide duplexes with improved in vitro potency and stability compared to unmodified small interfering RNA. J. Med. Chem. *48*, 901–904.

35. Manoharan, M., Akinc, A., Pandey, R.K., Qin, J., Hadwiger, P., John, M., Mills, K., Charisse, K., Maier, M.A., Nechev, L., et al. (2011). Unique gene-silencing and structural properties of 2'-fluoro-modified siRNAs. Angew. Chem. Int. Ed. Engl. *50*, 2284–2288.

36. Chiu, Y.L., and Rana, T.M. (2003). siRNA function in RNAi: a chemical modification analysis. RNA (New York, N.Y.) *9*, 1034–1048.

37. Layzer, J.M., McCaffrey, A.P., Tanner, A.K., Huang, Z., Kay, M.A., and Sullenger, B.A. (2004). In vivo activity of nuclease-resistant siRNAs. RNA (New York, N.Y.) *10*, 766–771.

38. Sakurai, K., Amarzguioui, M., Kim, D.-H., Alluin, J., Heale, B., Song, M-s, Gatignol, A., Behlke, M.A., and Rossi, J.J. (2011). A role for human Dicer in pre-RISC loading of siRNAs. Nucleic Acids Res. *39*, 1510–1525.

39. Schmitt, M., Hippeläinen, E., Raviña, M., Arango-Gonzalez, B., Antopolsky, M., Vellonen, K.S., Airaksinen, A.J., and Urtti, A. (2019). Intravitreal Pharmacokinetics in Mice: SPECT/CT Imaging and Scaling to Rabbits and Humans. Mol. Pharm. *16*, 4399–4404.

40. Sarkhel, S., Ramsay, E., Kontturi, L.-S., Peltoniemi, J., and Urtti, A. (2014). High-throughput in vitro drug release and pharmacokinetic simulation as a tool for drug delivery system development: Application to intravitreal ocular administration. Int. J. Pharm. *477*, 469–475.

41. Osborn, M.F., Coles, A.H., Biscans, A., Haraszti, R.A., Roux, L., Davis, S., Ly, S., Echeverria, D., Hassler, M.R., Godinho, B.M.D.C., et al. (2019). Hydrophobicity drives the systemic distribution of lipid-conjugated siRNAs via lipid transport pathways. Nucleic Acids Res. *47*, 1070–1081.

42. Ferguson, L.R., Dominguez, J.M., 2nd, Balaiya, S., Grover, S., and Chalam, K.V. (2013). Retinal Thickness Normative Data in Wild-Type Mice Using Customized Miniature SD-OCT. PLoS One *8*, e67265.

43. Vázquez-Domínguez, I., Anido, A.A., Duijkers, L., Hoppenbrouwers, T., Hoogendoorn, A.D.M., Koster, C., Collin, R.W.J., and Garanto, A. (2024). Efficacy, biodistribution and safety comparison of chemically modified antisense oligonucleotides in the retina. Nucleic Acids Res. *52*, 10447–10463.

44. Grainok, J., Utama, S., Chai, T., Ong, F., Champain, D., Lui, G., Tian, M., Thorne, M., Jackson, C., Sain, P., et al. (2024). PYC-001: A Promising RNA Therapeutic for Autosomal Dominant Optic Atrophy. In 2024 ARVO Annual Meeting Abstract, p. 5305.

45. Lai, C.M., Dunlop, S.A., May, L.A., Gorbatov, M., Brankov, M., Shen, W.Y., Binz, N., Lai, Y.K., Graham, C.E., Barry, C.J., et al. (2005). Generation of transgenic mice with mild and severe retinal neovascularisation. Br. J. Ophthalmol. *89*, 911–916.

46. Bhal, S.K., Kassam, K., Peirson, I.G., and Pearl, G.M. (2007). The Rule of Five Revisited: Applying Log D in Place of Log P in Drug-Likeness Filters. Mol. Pharm. *4*, 556–560.

47. Estupiñán, H.Y., Baladi, T., Roudi, S., Munson, M.J., Bost, J., Gustafsson, O., Velásquez-Ramírez, D., Bhatt, D.K., Hagey, D., Hekman, D., et al. (2025). Design and screening of novel endosomal escape compounds that enhance functional delivery of oligonucleotides in vitro. Mol. Ther. Nucleic Acids *36*, 102522.

48. Brown, K.M., Nair, J.K., Janas, M.M., Anglero-Rodriguez, Y.I., Dang, L.T.H., Peng, H., Theile, C.S., Castellanos-Rizaldos, E., Brown, C., Foster, D., et al. (2022). Expanding RNAi therapeutics to extrahepatic tissues with lipophilic conjugates. Nat. Biotech. *40*, 1500–1508.

49. Bienk, K., Hvam, M.L., Pakula, M.M., Dagnæs-Hansen, F., Wengel, J., Malle, B.M., Kragh-Hansen, U., Cameron, J., Bukrinski, J.T., and Howard, K.A. (2016). An albumin-mediated cholesterol design-based strategy for tuning siRNA pharmacokinetics and gene silencing. J. Control. Release *232*, 143–151.

50. Lorenz, C., Hadwiger, P., John, M., Vornlocher, H.-P., and Unverzagt, C. (2004). Steroid and lipid conjugates of siRNAs to enhance cellular uptake and gene silencing in liver cells. Bioorg. Med. Chem. Lett. *14*, 4975–4977.

51. Chen, S., Mao, Q., Cheng, H., and Tai, W. (2024). RNA-Binding Small Molecules in Drug Discovery and Delivery: An Overview from Fundamentals. J. Med. Chem. *67*, 16002–16017.

52. Zheng, Y., and Tai, W. (2020). Insight into the siRNA transmembrane delivery-From cholesterol conjugating to tagging. Wiley Interdiscip. Rev. Nanomed. Nanobiotechnol. *12*, e1606.

53. Gilleron, J., Querbes, W., Zeigerer, A., Borodovsky, A., Marsico, G., Schubert, U., Manygoats, K., Seifert, S., Andree, C., Stöter, M., et al. (2013). Image-based analysis of lipid nanoparticle-mediated siRNA delivery, intracellular trafficking and endosomal escape. Nat. Biotechnol. *31*, 638–646.

54. Dowdy, S.F. (2023). Endosomal escape of RNA therapeutics: How do we solve this rate-limiting problem? RNA (New York, N.Y.) *29*, 396–401.

55. Tai, W., Zhao, P., and Gao, X. (2020). Cytosolic delivery of proteins by cholesterol tagging. Sci. Adv. *6*, eabb0310.

56. Guo, Y., Terazzi, E., Seemann, R., Fleury, J.B., and Baulin, V.A. (2016). Direct proof of spontaneous translocation of lipid-covered hydrophobic nanoparticles through a phospholipid bilayer. Sci. Adv. *2*, e1600261.

57. Mix, K.A., Lomax, J.E., and Raines, R.T. (2017). Cytosolic Delivery of Proteins by Bioreversible Esterification. J. Am. Chem. Soc. *139*, 14396–14398.

58. Sangsuwan, R., Tachachartvanich, P., and Francis, M.B. (2019). Cytosolic Delivery of Proteins Using Amphiphilic Polymers with 2-Pyridinecarboxaldehyde Groups for Site-Selective Attachment. J. Am. Chem. Soc. *141*, 2376–2383.

59. Zhao, P., Song, S., He, Z., Dai, G., Liu, D., Shen, J., Asakawa, T., Zheng, M., and Lu, H. (2024). Development of a novel cholesterol tag-based system for trans-membrane transport of protein drugs. Biosci. Trends *17*, 503–507.

60. Park, S., Lee, Y.W., Oh, J., Kim, S.J., Lee, S., and Lee, H.Y. (2022). Pharmacokinetic evaluation of radiolabeled intraocular anti-CLEC14a antibody in preclinical animal species and application in humans. Clin. Transl. Sci. *15*, 2938–2946.

61. Del Amo, E.M., and Urtti, A. (2015). Rabbit as an animal model for intravitreal pharmacokinetics: Clinical predictability and quality of the published data. Exp. Eye Res. *137*, 111–124.

62. Solano, E.C.R., Kornbrust, D.J., Beaudry, A., Foy, J.W.D., Schneider, D.J., and Thompson, J.D. (2014). Toxicological and pharmacokinetic properties of QPI-1007, a chemically modified synthetic siRNA targeting caspase 2 mRNA, following intravitreal injection. Nucleic Acid Ther. *24*, 258–266.

63. Del Amo, E.M., Rimpelä, A.K., Heikkinen, E., Kari, O.K., Ramsay, E., Lajunen, T., Schmitt, M., Pelkonen, L., Bhattacharya, M., Richardson, D., et al. (2017). Pharmacokinetic aspects of retinal drug delivery. Prog. Retin. Eye Res. *57*, 134–185.

64. Hua, L., Wang, D., Wang, K., Wang, Y., Gu, J., Zhang, Q., You, Q., and Wang, L. (2023). Design of Tracers in Fluorescence Polarization Assay for Extensive Application in Small Molecule Drug Discovery. J. Med. Chem. *66*, 10934–10958.

65. Chen, C., Ridzon, D.A., Broomer, A.J., Zhou, Z., Lee, D.H., Nguyen, J.T., Barbisin, M., Xu, N.L., Mahuvakar, V.R., Andersen, M.R., et al. (2005). Real-time quantification of microRNAs by stem-loop RT-PCR. Nucleic Acids Res. *33*, e179.

66. Chen, L., Bosmajian, C., and Woo, S. (2024). A highly sensitive stem-loop RT-qPCR method to study siRNA intracellular pharmacokinetics and pharmacodynamics. Biol. Methods Protoc. *9*, bpae029.

67. Cameron, E.G., Xia, X., Galvao, J., Ashouri, M., Kapiloff, M.S., and Goldberg, J.L. (2020). Optic Nerve Crush in Mice to Study Retinal Ganglion Cell Survival and Regeneration. Bio. Protoc. *10*, e3559.